

# **3DMEMS for small-scale robotics and mechatronics**

Final Report

PI: Sarah Bergbreiter

31 May 2019

5000 Forbes Ave  
Carnegie Mellon University  
Pittsburgh, PA 15213  
[sbergbre@andrew.cmu.edu](mailto:sbergbre@andrew.cmu.edu)

## **Summary of Contributions**

This report details the exploration of new materials, fabrication processes, and designs to enable 3D actuators and sensors at the microscale toward small-scale robotic systems. The work and results shown here bring together insights from experimental studies, manufacturing, modeling, and simulation for microscale 3D systems. The ability to 3D print new materials was a crucial development in this work, especially with regards to the combination of multiple materials for complex systems. Another key component of this work was the new fabrication processes and designs developed to create functional 3D printed components. The results of these experiments will allow these actuators and sensors to be incorporated into more complex systems in the future. Finally, as a continuation of previous work on mobility at small scales, we compiled much of the information that we had collected into a review article on sub-gram robotics that is summarized at the end of this report. The primary contributions of this work are summarized as follows.

- Sacrificial ink developed for 2-photon photolithography (2PP) printing in Nanoscribe
- Preliminary results on a minimally damped PDMS ink and shape memory polymer ink
- The first microfabrication process combining 3D printed actuators and 3D printed mechanisms
- Experimental process and results to determine process limitations of sputtering on 3D printed structures
- Actuated mechanisms using 3D printing and sputtering technique
- A review of existing robots and what is required for autonomy in sub-gram legged robots including power and actuation that will inform future design of 3D microactuators and sensors

More detail on this work is shared below and several paper drafts or finalized papers are attached. In addition, as evidenced by the address on this report, Prof. Bergbreiter recently moved her lab from the University of Maryland to Carnegie Mellon University (CMU). The majority of this work was completed at CMU.

## **Research: New Materials for microscale 3D printing**

The focus of the early portions of this project have been on expanding the materials toolbox for microscale 3D printing. Much of the work from this portion of the project is still in preparation for publishing so results are not final. Three materials were targeted:

- a sacrificial material that could be printed and washed away to create more complex 3D structures,
- a soft material without the significant damping of the previously printed soft material,
- and a functional shape memory polymer.

Results from each material system are presented below.

### Sacrificial Ink

During some of our early work into printing small scale actuators and sensors, we came to the conclusion that it would be incredibly beneficial to have a water soluble sacrificial material to print structural materials around and on top of. The alternative is significant anchoring that can be challenging to break and remove at these scales. As such we took inspiration from the support materials available on many commercial multi-jet printers (e.g., Stratasys) and adapted these materials for use in 2PP printing. The formulation tested includes SUP706 support material from Stratasys (a proprietary formulation), polyethylene glycol di-acrylate (PEGDA, Sigma Aldrich), Irgacure 369 (Omnicure, a photoinitiator), and Genocure ITX (Rahn USA Corp, a second photoinitiator). Three different inks were tested with different ratios of SUP706 support material and PEGDA as listed below.

**Table 1. Ink concentration of SUP706 support material (Stratasys) and PEGDA (Sigma-Aldrich)**

	SUP706 (% by wt.)	Cross-linker as PEGDA (% by wt.)
<b>SUP-0</b>	100	0
<b>SUP-2.5</b>	97.5	2.5
<b>SUP-5</b>	95	5

1% Irgacure 369 and 0.3% Genocure ITX with respect to total ink weight were then dissolved by stirring at room temperature. 3D printing was performed using the NanoScribe Photonic Professional GT using oil immersion mode with a 63x objective lens. Ultimately we would like to use this in DiLL configuration (in which the objective is dipped into the ink) but we are limited to oil immersion while we determine the compatibility of this ink with the objectives. A laser power of 37.5 mW and scan speed of 1250 – 10000  $\mu\text{m}/\text{s}$  were used followed by a development step in PGMEA for 20 min, an IPA wash for 1 min, and a dry at room temperature.

To start, we printed cubes that were 30  $\mu\text{m}$  on a side with the SUP-0 material. Interestingly, the measured height of these cubes was only half of the designed height at 15  $\mu\text{m}$ .

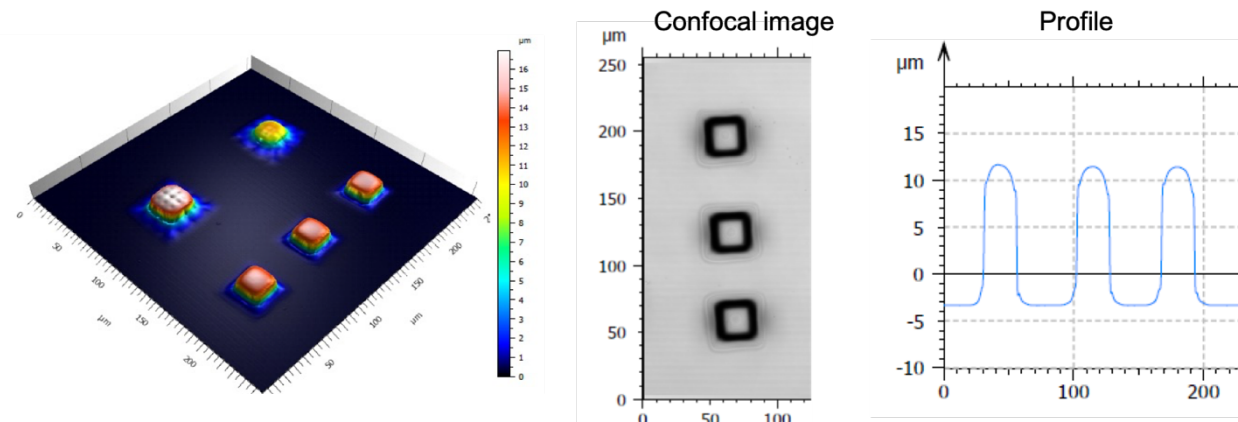


**Figure 1. 3D printed structures using sacrificial ink with 0% cross-linker (PEGDA).**

To measure the effect of cross-linker concentration and scan speed on the final cube height, we varied scan speed from 1,250 to 10,000  $\mu\text{m/s}$  and used the three concentrations in Table 1 above. Two different structures were tested including a  $30 \times 30 \times 30 \mu\text{m}^3$  cube structure tested above as well as a woodpile structure  $40 \times 40 \times 40 \mu\text{m}^3$  in size. The results are provided below indicating that a slow scan speed and higher percentage cross-linker provide structures closest to the designed size. It should be noted though that the wood-pile structure is still not close to  $40 \mu\text{m}$  in height and this is being investigated further.

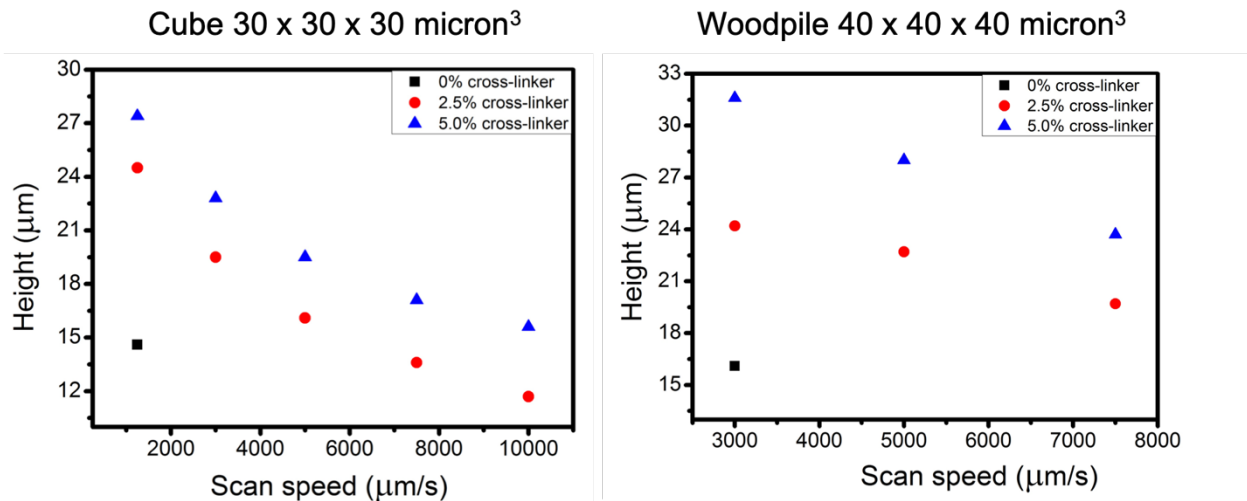


**Figure 2.** Varying cross-linker concentration and scan speed.

A confocal image with overlaid heightmap is also provided for structures using 5.0% cross-linker at slower scan speed. This image makes it clear that this combination resulted in better resolution of the printed structures.

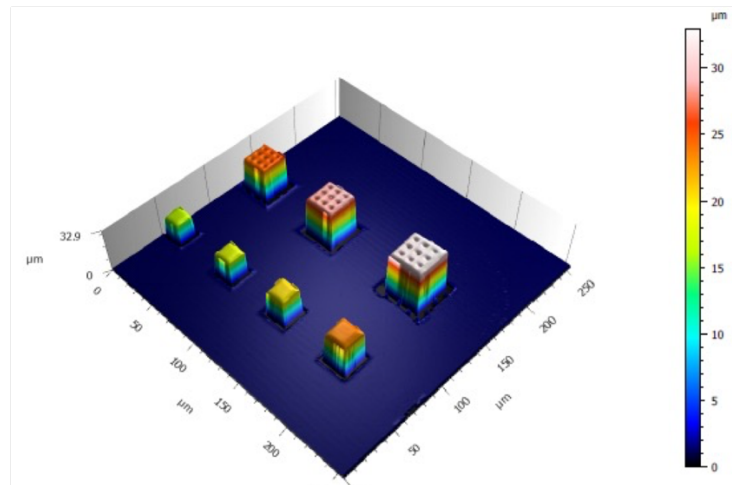


**Figure 3.** Addition of 5% cross-linker resulted in better resolution of the printed structures.

The next step was to test the solubility of the sacrificial ink. A key contribution of this ink is the ability to wash away the ink without damaging the structural material (e.g., IP-S) that would be supported by the sacrificial material. As an early test, 30  $\mu\text{L}$  of sacrificial ink with 5% cross-linker was polymerized on a glass slide using 395 nm UV light for 1 min. A support cleaning

solution was made by dissolving 2% NaOH and 1% sodium meta silicate by weight in distilled water through stirring. The polymerized sacrificial ink was placed in the support cleaning solution and visibly observed after 30 min, 45 min, and 60 min. After 60 min, it was clear that the polymerized ink dissolved completely.

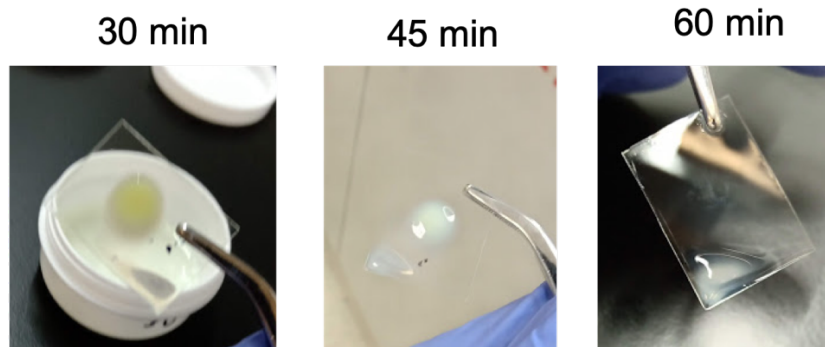


Figure 4. Sacrificial material being dissolved by the cleaning solution.

In a similar test, 30  $\mu$ L of two different structural materials, IP-S and IP-L (NanoScribe) were polymerized on a glass slide using 395 nm UV light for 1 min. This polymerized material was then placed in the support cleaning solution to visibly observe any changes and look for delamination. After 120 min, the material visibly looked the same and did not delaminate indicating that the two materials have a high selectivity in the cleaning solution.



Figure 5. Structural materials remain after immersion in the cleaning solution indicating high selectivity between the structural material and sacrificial material.

Further tests are currently being conducted to demonstrate the ability to print novel structures and shapes without anchoring through use of this new sacrificial material and the work will be written up into a journal paper for a journal such as Advanced Functional Materials or ACS Applied Materials & Interfaces.

#### PDMS Ink

Previous work on this project demonstrated the printing of a soft material, urethane di-acrylate (UDA), along with more conventional materials in the Nanoscribe (this paper was recently accepted with minor revisions to Soft Robotics and is attached). However, the UDA has significant viscoelasticity and damping which reduces its utility for microrobotic mechanisms. In order to address this in future work, we began working on a PDMS ink formulated using a copolymer of methacryloxypropyl poly(dimethyl siloxane) and poly(dimethyl siloxane) (RMS-044, Gelest), methacryloxypropyl poly(dimethyl siloxane) (DMS-R31, Gelest), Irgacure 369

(Omnicure) and Genocure ITX (Rahn USA Corp.). The DMS-R31 and RMS-044 were mixed in a ratio of 9:1. 1% Irgacure and 0.3 % Genocure with respect to total ink weight were dissolved using stirring. Oil immersion was used once again with the 63x objective, but xylene was used as a developer after PGMEA was found to be unsuccessful. This xylene develop step was 30 min and then the structures were immersed in IPA for 1 min followed by a room temperature drying step.

One of the key problems encountered thus far as been structure height. Short < 10 mm structures develop OK, but larger structures (e.g., the octopus in Fig. 6) have still not been printed and developed successfully.

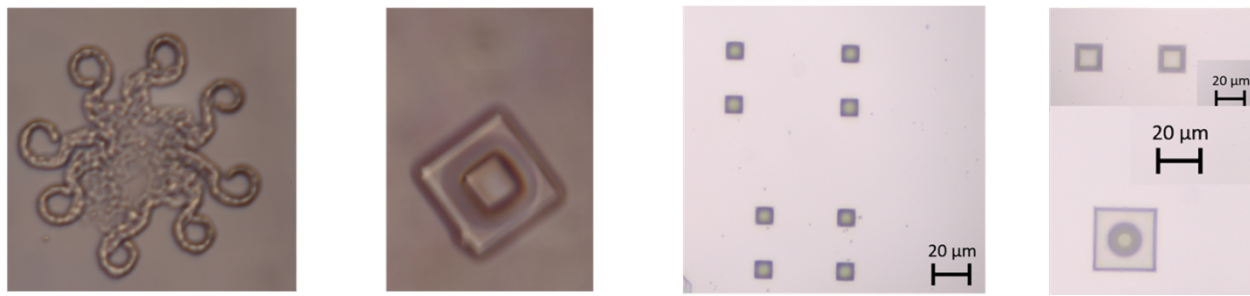


**Figure 6. 3D printed structures using PDMS ink**

#### *Shape Memory Polymer Ink*

Finally, one of the goals of this work was to print functional materials at the microscale. To start, we have begun investigating shape memory polymers as these have successfully been printed using larger scale stereolithography techniques. Thus far, we have been unsuccessful with the several formulations that we have tried, but they are listed here for convenience.

A variety of ratios of Benzyl methacrylate (BMA, Sigma Aldrich), polycaprolactone (PCL, Sigma Aldrich), polycaprolactone methacrylate (PCLMA), Butyl acrylate (BA, Sigma Aldrich), aliphatic urethane diacrylate (AUD, Ebecryl 8413, Allnex), and polyethylene glycol diacrylate (PEGDA)/polyethylene glycol dimethacrylate (PEGDMA) were used along with different photoinitiators – Irgacure 369 (Omnicure) and Genocure ITX (Rahn USA Corp.). The combinations tested thus far are listed in the tables below.

**Table 2. Set 1 of SMP trials**

BMA:AUD or BA:AUD	PCL
1:1	5 %
1.5:1	5 %
2:1	5 %
2.5:1	2.5 and 5 %
3:1	5 %

**Table 3. Set 2 of SMP trials**

BMA:PCLMA	Irgacure 369	Genocure ITX
9:1	2%	0.3%
8:2	2%	0.3%
7:3	2%	0.3%
6:4	2%	0.3%
BMA:PEG (DA/MDA)	PCL	
3:1	5%	

### **Research: Microscale Actuator and Sensor Design by Sputtering on 3D Printed Structures**

Effective microrobot locomotion and manipulation will require forces and torques to be applied in three dimensions. However, traditional MEMS processing is inherently 2D; creating 3D architectures requires design in 2D followed by manual assembly or hinges and flexural joints to fold 3D structures. One goal of this work was to demonstrate a simple fabrication process for actuated 3D mechanisms fabricated using a 2-photon photolithography (2PP) process and a subsequent sputtering process. Two difference actuators are shown -- a thermal actuator design is used to electrically control the actuator within complex 3D printed mechanisms and a preliminary electrostatic actuator is also highlighted. Finally, some preliminary capacitive sensor designs are demonstrated.

#### *Thermally actuated 3D mechanisms*

The fabrication process for the thermally actuated mechanisms consists of two steps, 3D printing and aluminum sputtering, as shown in Figure 7. First, a drop of IP-S photoresist was put on an ITO coated glass substrate. The desired structure is printed by 2PP printing, carried out by a NanoScribe Photonic Professional GT using the Dip-In Laser Lithography mode. In this work all samples were printed with a 25x objective lens, a laser power of 37.5 mW, and a scan speed of  $40,000 \mu\text{m}\cdot\text{s}^{-1}$ . Printed structures were developed in PGMEA for 20 min, immersed in isopropyl alcohol for 1 min, and dried at room temperature (Figure 7(a)). After printing, the resulting structures were sputtered with approximately 60 nm of aluminum (Perkin Elmer 2400-8L). Aluminum was sputtered over the actuator for electrical conductivity, and the actuators and mechanisms were designed to be electrically isolated from the substrate using 10  $\mu\text{m}$  clearance gaps (Figure 7(b)).

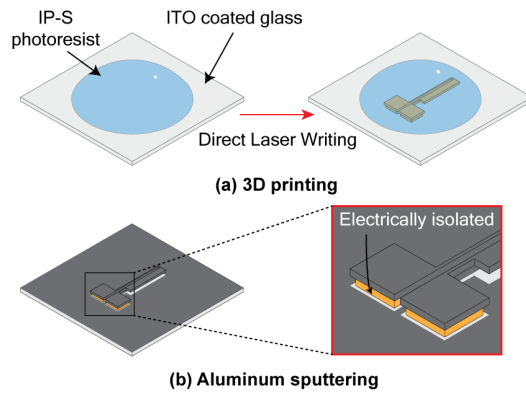


Figure 7. Schematic of fabrication process

Figure 8(a) shows two-beam thermal actuators in various configurations by printing a rotated version of the actuator ( $0^\circ$ ,  $25^\circ$ , and  $90^\circ$  rotations). The dimensions of the actuator are shown in Figure 8(b).

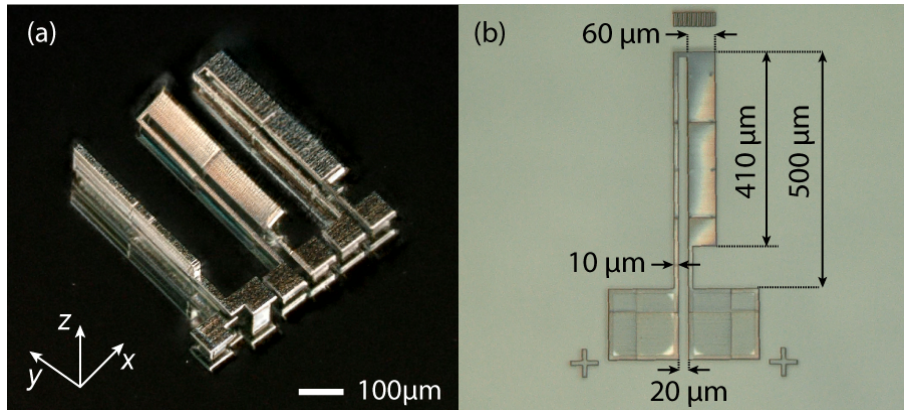


Figure 8. (a) A digital microscope image of fabricated 2-beam thermal actuator in various configurations, (b) the dimensions of the thermal actuator.

The actuators were first characterized without integrated mechanisms. Figure 9 shows the displacement of the planar thermal actuator with respect to applied power. When more than 12 mW was applied, the sputtered aluminum cracked, causing a loss of electrical conductivity. The bandwidth of the actuator is presented in Figure 10. A 50% duty cycle square wave with a 1V peak-to-peak voltage (Vpp) was applied. After 55 Hz, the displacement decreased to 70% of its maximum value. While not the most efficient actuators, they are able to actuate at reasonable frequencies for microrobot and mechatronic actuation.

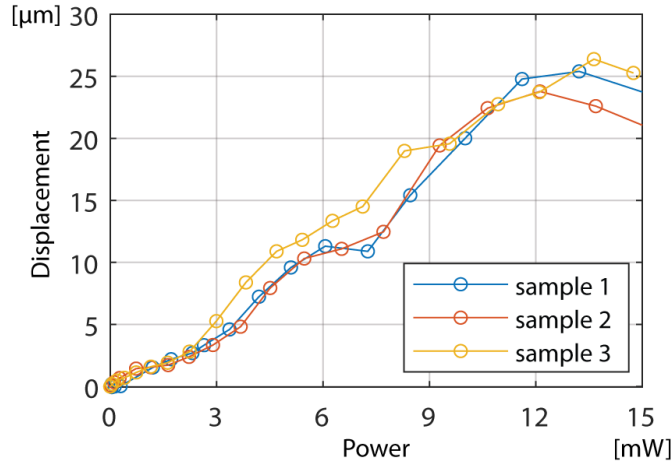


Figure 9. Voltage to power experimental result of the 2-beam thermal actuator; sample size = 3

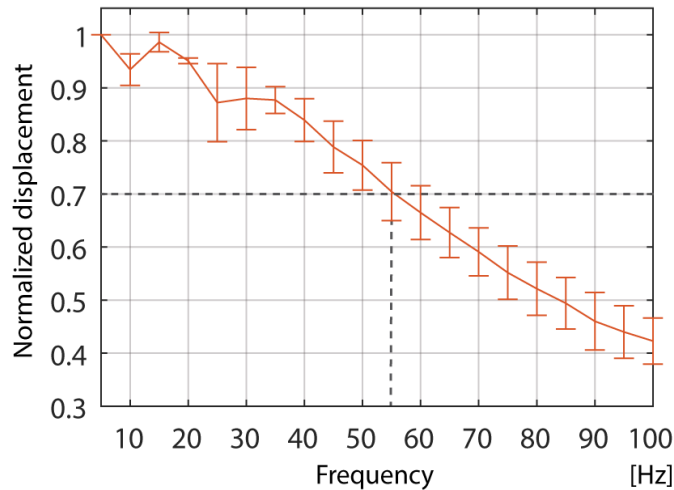


Figure 10. Bandwidth experimental result of the 2-beam thermal actuator; error bars show standard deviation for a sample size of 2

Most importantly, two actuated mechanisms were used to demonstrate the novel fabrication method: (1) A 90° rotated actuator, which generates both forward and vertical force, is printed with a compliant mechanism for flapping wing motion. Figure 11(b) shows the movement of the wing tip with a 2 Vpp square wave applied. (2) A rotary motor (Figure 12) was designed with four 25° rotated actuators arranged in a circular pattern to drive a rotor. The rotor is printed separately and manually placed on the actuators. Two independent 60% duty cycle square waves (1.6 Vpp, 5 Hz, and 180° phase difference) were applied to the opposite actuator pairs. Figures 6(c) and (d) show the rotor rotating 14° in 2.4 s.

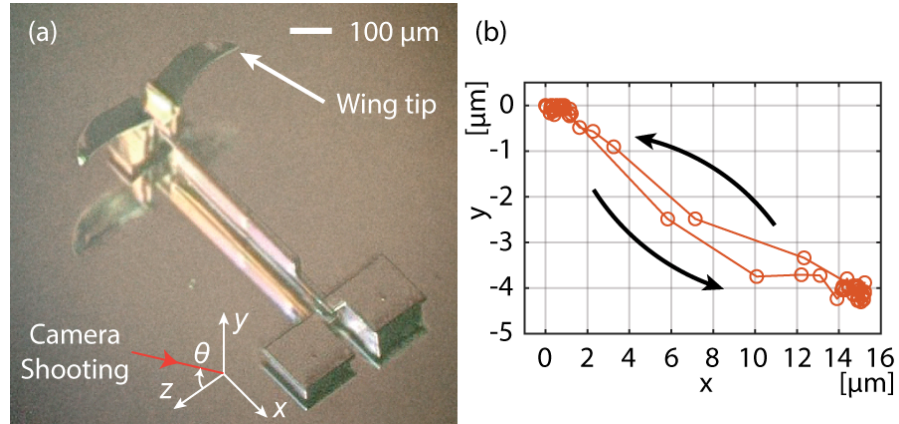


Figure 11. A flapping wing mechanism (a) a digital microscopic image of the mechanism (b) a plot of wing tip motion. The movement was recorded with a camera with an infinity lens ( $\theta = 35^\circ$ )

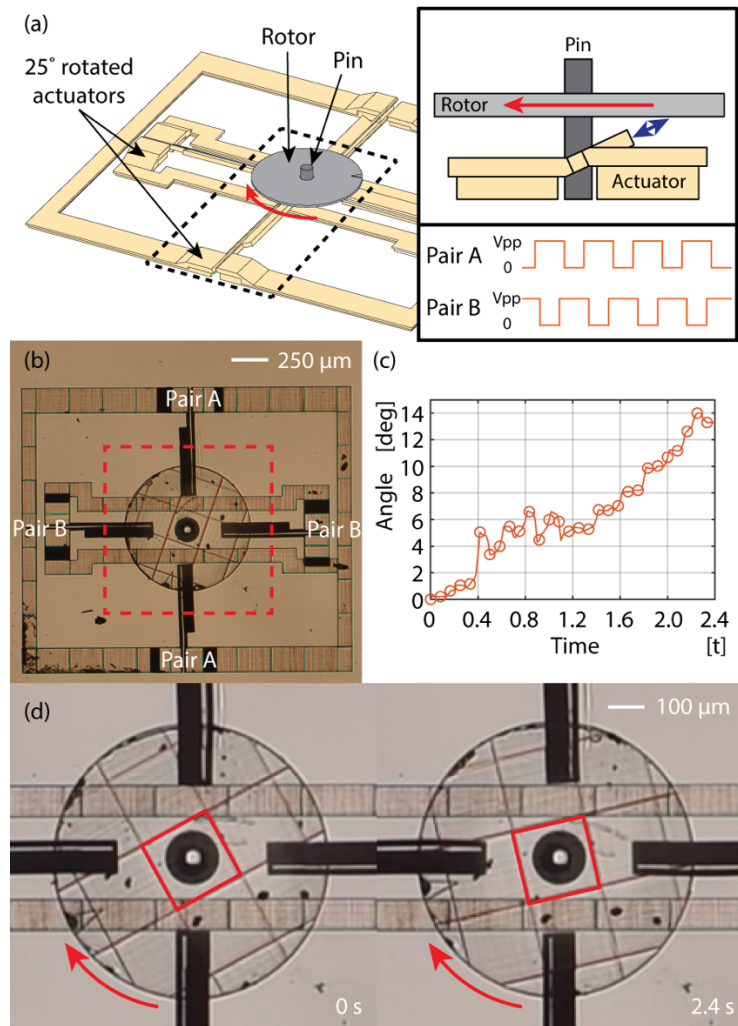


Figure 12. A rotary motor (a) 3D CAD image of the motor, (b) an optical microscopic image of the motor, (c) a plot of the rotor angle respective to time, (d) video stills of the motor

Design improvements are required to further improve the functionality of both mechanisms, but they already demonstrate the potential of this novel process. This work along with some more recent improvements is currently being written up for submission to Science Robotics or JMEMS (TBD pending on-going experiments).

#### *Electrostatic actuation*

To demonstrate the ability to create efficient actuators in this process, we have also recently fabricated some preliminary electrostatic actuators. To start, we fabricated a standard comb-drive actuator (Figure 13). In this actuator, the finger length is 70  $\mu\text{m}$  and initial overlap was 20  $\mu\text{m}$ . The displacement was 17  $\mu\text{m}$  when 160 V was applied, but the actuator became unstable at 170 V. According to a simple comb drive analytical model, the displacement should be 50  $\mu\text{m}$  at 170 V indicating some additional friction due to anchoring or other unmodeled phenomena. A video can also be found here: <https://bit.ly/2QOqh4v>.

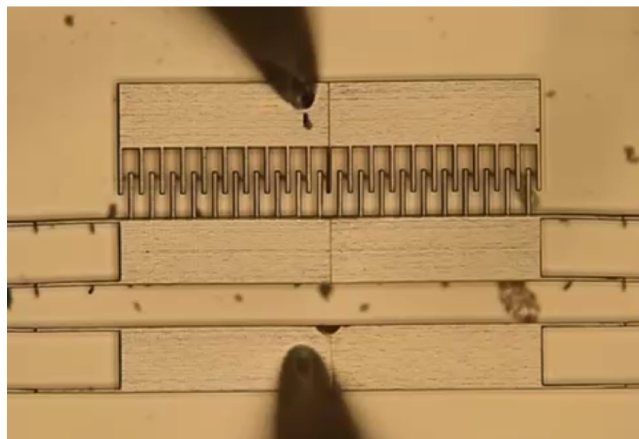


Figure 13. 3D printed electrostatic actuator

#### *Capacitive sensing*

Finally, sensors are a key part of 3D MEMS and we started looking at similar structures to the comb drive actuator as capacitive sensors. However, these have not been systematically tested as of yet although we do not anticipate any major differences between these sensors and silicon based sensors other than possible damping due to anchoring.

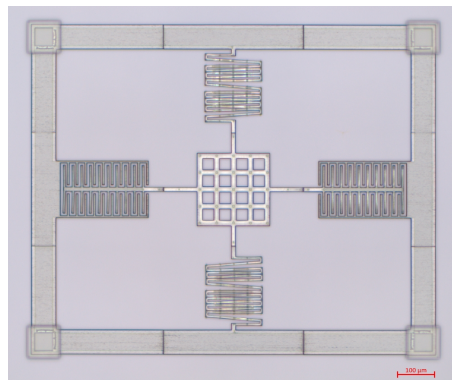


Figure 14. Capacitive sensor for possible at-scale rat whisker.

## **Research: Sub-Gram Legged Robots**

Very little is known about locomotion below the scale of 1 gram, but robots at this size scale would be able to carry reasonable sensor payloads including imaging sensors. As a continuation of earlier work on this project, we compiled much of the previous work that we had done into a review and perspective on legged locomotion at sub-gram scales. This compilation of data is highly valuable toward the work on this project as well in terms of specifying the requirements of sensors and actuators for small-scale robotics. In addition, the visualization of existing data from robots and organisms (insects) highlights the substantial improvements that can be made in small scale robotics if the required mechanisms, sensors, actuators, and controllers can be integrated in useful ways. The entire database of robots evaluated as part of this study can be found at <http://ter.ps/botsandbugs>.

We started by looking at the overall autonomy of the terrestrial robots at these size scales and robots were ranked by an autonomy score defined as the Boolean sum of presence (1) or absence (0) of onboard power, onboard control, and onboard sensing. Existing robots are plotted in Figure X with respect to both mass and length scale; the large majority of existing robots scored a 0 indicating that they are simply actuated mechanisms while the robots with the highest autonomy score were typically large.

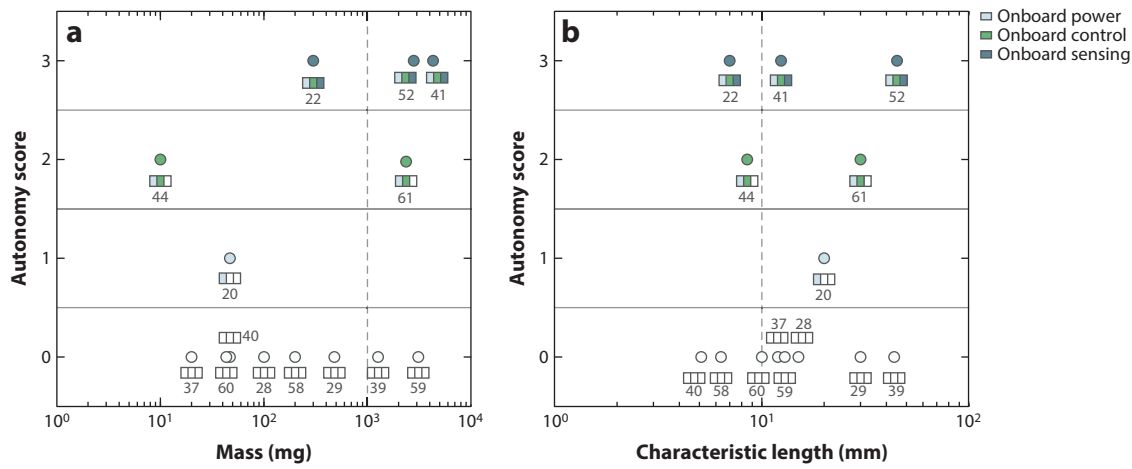
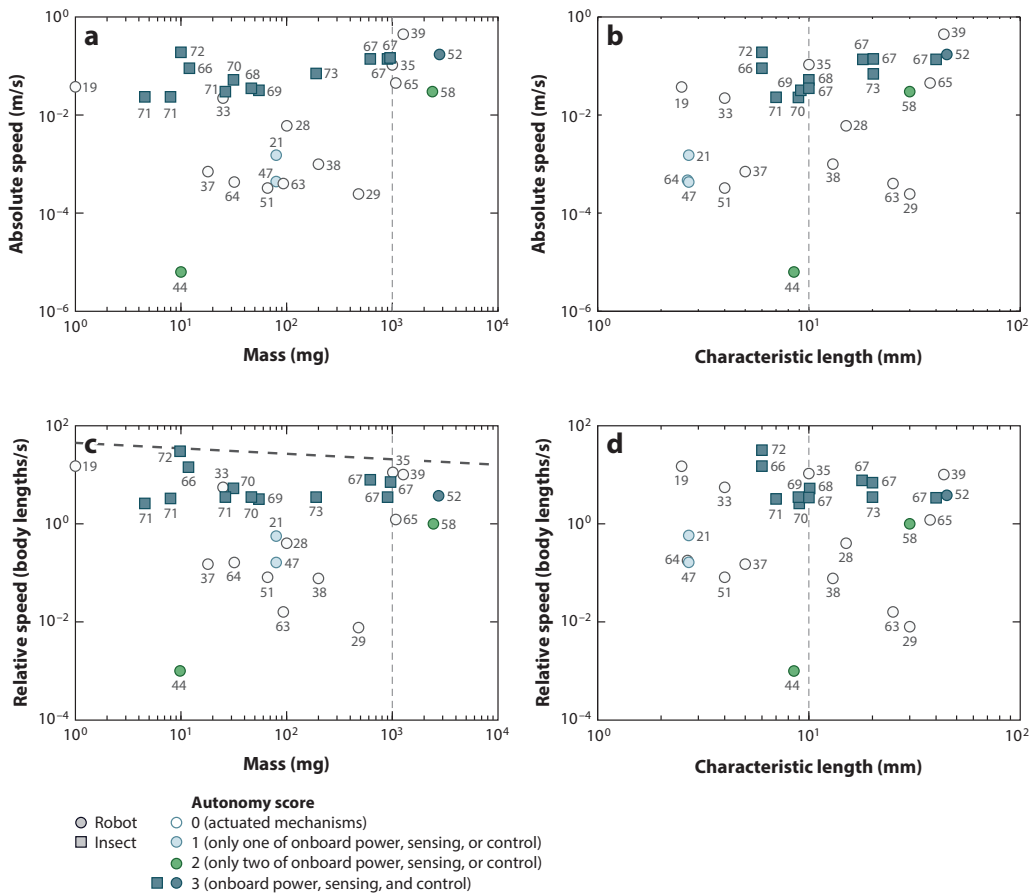
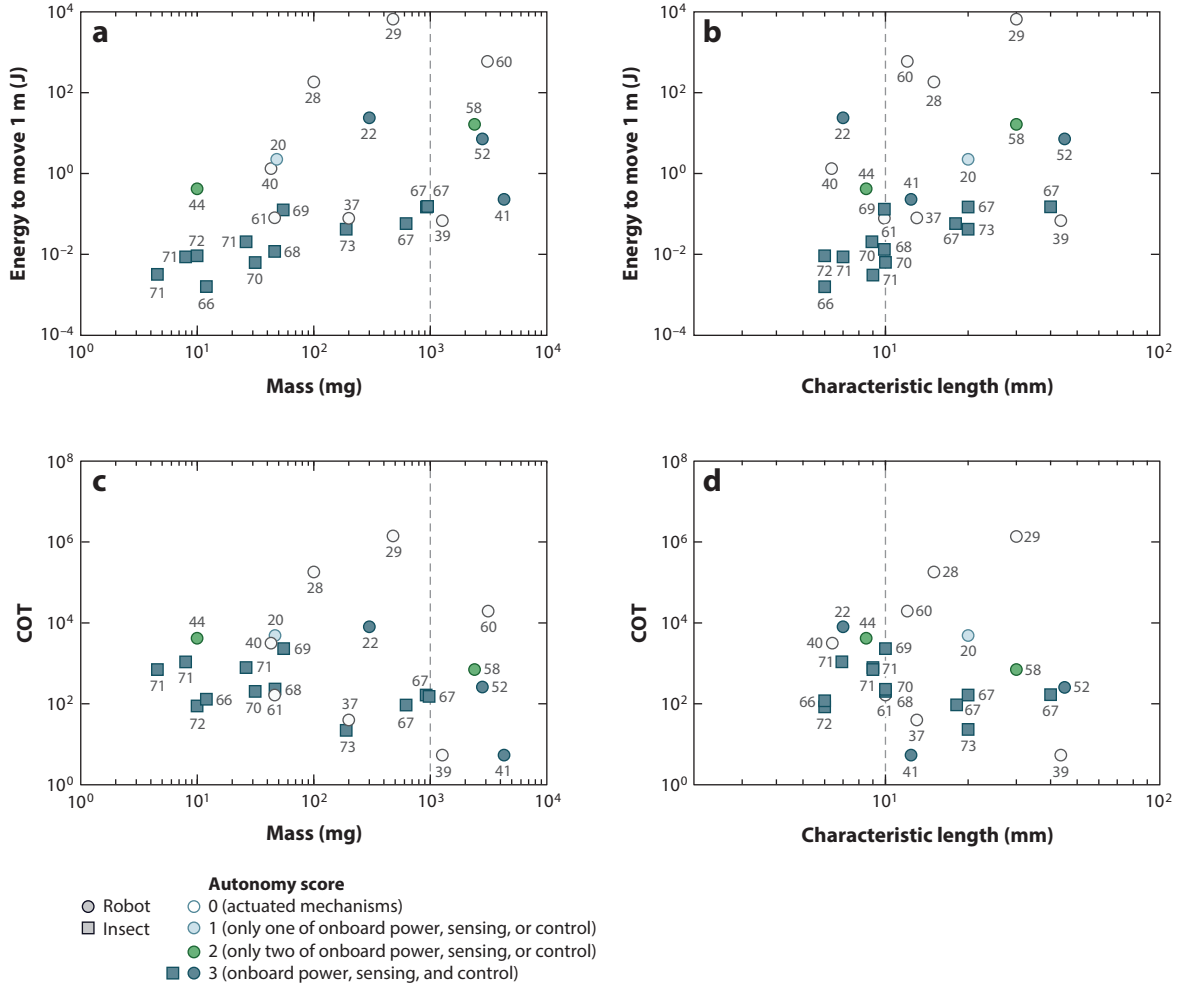


Figure 15. Autonomy score of existing robots found at <http://ter.ps/botsandbugs>

We also evaluated performance metrics for these existing robots to provide points of comparison between existing robots. Speed is an important one that is measured in the vast majority of papers (Figure X), but the energetic costs including energy to move 1 m and cost of transport are probably even more important when considering the components that would go into a small-scale robot as we are doing in this work (Figure X).



**Figure 16. Absolute and relative speeds of select legged robots (circles) and insects (squares). Citations are listed in the attached paper.**



**Figure 17.** The energy to move 1 m and cost of transport (COT) of select robots (circles) and insects (squares). Citations are provided in the attached paper.

By highlighting autonomy on these plots as well, it is clear that the robot data that are collocated with the insect data are the least autonomous; their tethered operation provides an artificially low energy for movement and COT. An important takeaway from these data and comparisons is that the energy required for locomotion in robots is still orders of magnitude higher than the energy required by similarly sized insects at scales below 1 g. This shows an efficiency gap between the robotic systems and insects and points toward research opportunities pursued in this work on integration of actuators and sensors in 3D microscale packages.

One of the primary conclusions of this work was the need to enable power autonomy through efficiencies and integration. Efficient actuators that could easily be integrated with complex mechanisms were identified as an important part of this work. A second conclusion was around enabling mobility autonomy through design and fabrication. Related to previous work done on this funding with printing of multiple materials, the suspension of insect exoskeletons often allows them to overcome obstacles and disturbances passively. The integration of microactuators and sensors with these multimaterial mechanisms without the requirement of assembly will be a critical contribution of this work going forward.

## **Group members supported**

- Dr. Dinesh Patel, post-doc Mechanical Engineering (picked up from collaboration with Prof. Shlomo Magdassi's lab at Hebrew University) – material and salary support
- Dr. Ryan St. Pierre, PhD Mechanical Engineering granted May 2018, converted to post-doc – primarily material support
- Sukjun Kim, PhD student in Mechanical Engineering, started at CMU in August 2018 – material support (on a fellowship this year)

## **Next Steps**

Now that we have 3D printed actuators through the sputtering process along with preliminary results from new materials, we look forward to integrating this work with past results on mobility to addressing power autonomy in small-scale robotics. As part of the next phase of this work, we will leverage some of our actuator designs with multi-material mechanisms to enable power autonomous robots.

In addition, Dr. Dinesh Patel will continue working on wrapping up the novel materials printing in the 2PP process. The ability to translate the wide variety of materials available in larger scale stereolithography systems to the Nanoscribe is still a goal of this work as it provides a large materials toolbox to design in.

Finally, multiple publications are in the final stages of editing and writing as shown below.

## **Publications**

\* Publications with an asterisk are attached in draft or final form

*(follow-on from previous project)*

- \* **R. St. Pierre, W. Gosrich, and S. Bergbreiter**, “A 3D-printed 1 mg legged microrobot running at 15 body lengths per second,” Hilton Head 2018 Workshop, June 3-7, 2018. **Best Paper Award!**
- \* **M. Soreni-Harari, R. St. Pierre, C. McCue, K. Moreno, and S. Bergbreiter**, “Multimaterial 3D printing for microrobotic mechanisms,” accepted to Soft Robotics, 2019.

*(current work in report)*

- \* **R. St. Pierre and S. Bergbreiter**, “Toward Autonomy in Sub-Gram Terrestrial Robots,” Annual Review of Control, Robotics, and Autonomous Systems, v. 2, n. 1, May 2019, p. 231-252.
- \* **S. Kim, C. Velez-Cuervo, D. Patel, G. Smith, and S. Bergbreiter**, “3D printed actuated mechanisms for microrobots,” abstract attached, in preparation for Science Robotics or JMEMS.
- D. Patel, C. Velez-Cuervo**, and S. Bergbreiter, “High selectivity sacrificial inks for 2PP printing,” in preparation for ACS Applied Materials and Interfaces.